Electronic structure and electric-field gradient analysis in $CeIn_3$

S. Jalali Asadabadi*

Department of Physics, Faculty of Science, and Research Center for Nanosciences and Nanotechnology, University of Isfahan (UI), Hezar Gerib Avenue, Isfahan 81744, Iran

(Received 9 September 2006; revised manuscript received 27 March 2007; published 31 May 2007)

Electric field gradients (EFGs) were calculated for the $CeIn_3$ compound at both In and Ce sites. The calculations were performed within the density functional theory (DFT) using the augmented plane waves plus local orbital (APW+lo) method employing the so-called LDA+U scheme. The $CeIn_3$ compound was treated as nonmagnetic, ferromagnetic, and antiferromagnetic cases. Our result shows that the calculated EFGs are dominated at the Ce site by the Ce-4*f* states. An approximately linear relation is intuited between the main component of the EFGs and the total density of states (DOS) at Fermi level. The EFGs from our LDA+U calculations are in better agreement with experiment than previous EFG results, where appropriate correlations had not been taken into account among 4*f*-electrons. Our result indicates that correlations among 4*f*-electrons play an important role in this compound and must be taken into account.

DOI: 10.1103/PhysRevB.75.205130 PACS number(s): 71.20.−b, 71.28.+d, 76.80.+y, 71.27.+a

I. INTRODUCTION

Hyperfine interactions provide sensitive physical quantities such as electric field gradients (EFGs), which can be used to shed light experimentally[1,2] and theoretically[3,4] into the electronic states of materials. In this paper we have focused on $CeIn_3$ as an interested system composed of strongly correlated 4*f*-electrons. It is a cubic heavy-fermion (HF) local moment antiferromagnetic (LMAF) system at ambient pressure with a Néel temperature of 10.1 K.[5] This concentrated Kondo compound exhibits[6] various fascinating and unexpected physical properties. The various properties of this heavy fermion originate from the fact that one cannot assign a definite localization to the 4*f*-states, irrespective of the applied conditions to the compound. The unexpected physical behavior may be then attributed to the degree of localization of the 4*f*-electrons, i.e., the positions of the 4*f*-density of states (4*f*-DOS) with respect to the Fermi level. The position of the 4*f*-DOS demonstrates the degree of hybridization between localized 4*f* and valence bands. The EFG quantity is extremely sensitive to the anisotropic charge distributions of the core electrons[7] as well as to the aspherical electron density distribution of valance electrons,[8] and as a result to the valance electronic structure. The EFG, thereby, can serve as a powerful gauge for measuring such a degree of localization.

Rusz *et al.*[9] very recently calculated Fermi surfaces of $CeIn_3$ regardless of its antiferromagnetic ordering. Their calculations were performed in the localized extreme limit within the open core treatment.[10,11] On the other delocalized extreme limit two individual groups[3,4] calculated the EFG at the In site in this compound. The calculations of the former[3] and latter[4] groups were performed, respectively, in the antiferromagnetic and nonmagnetic phases employing a similar method of the full-potential linearized augmented plane waves (FP-LAPW).[12]

In this paper, we have examined whether one can, using an intermediate way, improve the previous results of the localized and delocalized limits. For this purpose, we have employed the LDA+U scheme[13–15] and then calculated the EFGs at both In and Ce sites. The more advanced method of augmented plane waves plus local orbital (APW+lo)[16,17] were used to linearize the energies. This is a report of the EFG calculations within the LDA+U scheme employing the APW+lo method for this compound. Our spin-polarized calculations demonstrate nonzero EFG at the Ce site in the presence of spin-orbit coupling. The cubic symmetry of the Ce site explains why the EFGs were less significant to be previously reported. Nevertheless, a result has emerged that shows the EFGs are dominated at the Ce site by 4*f*-states and not as usual by *p*-states. The goal of this work is to illustrate an approximately linear relationship between the values of EFG and density of states (DOS) at Fermi level (E_F), viz. $\mathrm{EFG} \propto \mathrm{DOS}(E_F)$. We also aim to justify the tendency of the 4*f*-electrons in the ground state of the antiferromagnetic $CeIn_3$ compound to show their degree of localization. We have also found that correlations among 4*f*-electrons influence semicore states of 5*p*-Ce.

II. DETAILS OF THE CALCULATIONS

All the calculations in this work were performed in the framework of the density functional theory[18,19] (DFT). We have taken the generalized gradient approximation[20] (GGA) into account for the exchange-correlation functional. We have employed the full-potential augmented plane waves plus local orbital (APW+lo) method[16,17] as embodied in the WIEN2K code.[21] The muffin-tin radii (R_{MT}) were chosen to be 2.2 and 2.8 Å for the In and Ce atoms, respectively. It has been allowed to be the 4*s*4*p*4*f* orbitals of the Ce and 5*d*6*s* orbitals of In in the valance states. The expansion of the wave functions inside the spheres in lattice harmonics and in the interstitial region in plane waves were cut off by the maximum eigenvalue of $l_{\max}=10$ and the $R_{MT}K_{\max}=7$, respectively. The cutoff for the Fourier expansion of the charge density and potential was taken to be $G_{\max}=16\sqrt{\mathrm{Ry}}$. We used a mixing parameter of 0.001 in the Broyden's scheme to reduce the probability of occurrence of the spurious ghost-bands. A mesh of 165 special *k* points was taken in the irreducible wedge of the first Brillioun zone, which corresponds

 ©2007 The American Physical Society

to the grids of $18\times18\times18$ in the scheme of Monkhorst-Pack.[22] In order to perform the calculations nearly in the same accuracy for the case of a magnetic supercell compared to the nonmagnetic unit cell, the mesh of k points was reduced to 121 corresponding to $9\times9\times9$ grids. We diagonalized a spin-orbit coupling (SOC) Hamiltonian in the space of scalar relativistic[23] eigenstates using a second-variational procedure[24] imposing the (111) direction on the Ce magnetic moments within a cutoff energy of 3 Ry. In order to take into account strong correlations of $4f$ Ce states, we have used the LDA+U method.[13–15] Here, we have used a value of 6.2 eV for the U parameter of Ce in $CeIn_3$.[25] Another input parameter for the LDA+U calculation is the exchange integral J. Here, we have used 0.7 eV for the J value. This J parameter can be derived using the values of 8.34, 5.57, and 4.12 eV for the F^2, F^4, and F^6 Slatter integrals,[26] respectively, within the following expression, which is valid for the f electrons:

$$J=\frac{1}{3}\left(\frac{2}{15}F^2+\frac{1}{11}F^4+\frac{50}{429}F^6\right)\approx 0.69\ \text{eV}. \qquad (1)$$

Finally, since the factor of $(U\text{-}J)$ appears in the total energy of the LDA+U method instead of U and J individually, we set J to zero, and let U be equal to the effective value[27] of $U_{eff}=U-J=5.5$ eV.

III. CHEMICAL, MAGNETIC, AND ELECTRONIC STRUCTURES

A. Chemical structure

As shown in Fig. 1(a), $CeIn_3$ crystallizes in the space group of $Pm\bar{3}m$ with the binary-fcc prototype of $AuCu_3$. It is a cubic unit cell, where Ce atoms are located on the corners, and the In atoms on the middle of the surfaces. The point groups of Ce and In atoms are the cubic m-3m, and the noncubic $4/mmm$, respectively. The lattice parameter of the $CeIn_3$ was measured[28] to be 4.69 Å. We have used this chemical structure to simulate the nonmagnetic and ferromagnetic phases.

B. Magnetic structure

It has been experimentally observed that the cerium moments in this compound are aligned antiferromagnetically in adjacent (111) magnetic planes.[5] Therefore in order to simulate the antiferromagnetic situation, first the sides of the nonmagnetic unit cell were doubled as depicted in Fig. 1(b) in all three Cartesian xyz directions. We have preserved the space group of $Pm\bar{3}m$ for the new magnetic supercell. The preserved fcc symmetry of the magnetic supercell causes the number of atoms to be reduced in the primitive rhombohedral magnetic unit cell, see Fig. 1(c), compared to the conventional unit cell shown in Fig. 1(b). Second, we have imposed the antiferromagnetic ordering on the magnetic moments of Ce sites. The direction of the $4f$ spin in the ground state electron configuration of the Ce atom, i.e., $[Xe]4f^{\uparrow}5d^{\uparrow}6s^{\uparrow\downarrow}$, were exchanged, i.e., $[Xe]4f^{\downarrow}5d^{\uparrow}6s^{\uparrow\downarrow}$, alternatively with the ordering of $(\uparrow\downarrow)$ in the (111) direction as shown in Fig. 1(d).

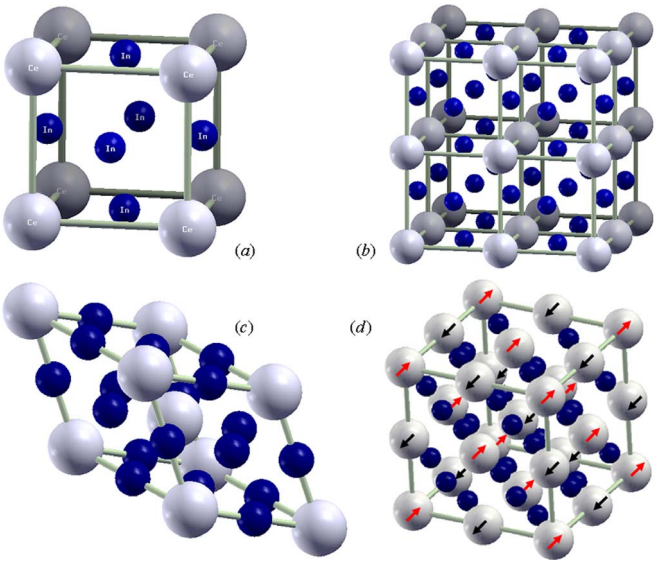

FIG. 1. (Color online) (a) Chemical unit cell of $CeIn_3$ in the $AuCu_3$ prototype having the lattice parameter of a=4.69 A. (b) Constructed conventional supercell with the symmetry of face-centered cubic ($Pm\bar{3}m$ space group) from the chemical unit cell by a factor of 2 as a number of chemical unit cells drawn in three directions of xyz Cartesian coordinates. (c) Primitive rhombohedral unit cell of the constructed conventional supercell. (d) Magnetic supercell imposing spin ordering of $(\uparrow\downarrow)$ to the Ce moments along the (111) axis.

C. Electronic structure

We have calculated the density of states (DOS) in the absence of both spin-polarization (SP) and spin orbit coupling (SOC). This calculation has been performed using the chemical structure; Fig. 1(a). This is what we call the nonmagnetic (NM) phase from now on. The SOC was then included in two individual steps. The calculations in the first step were performed including spin-orbit interactions among only Ce electrons. We refer to the results of this calculation by the name of "NM+SOC(only Ce)." The SOC was then, as the second step, included among the In electrons as well. We call it "NM+SOC" phase from now on. For sure, the SOC is included in both Ce and In atoms in the "NM+SOC" phase. Our calculated DOSs are in agreement with the previous calculations[3] and we avoid repeating them here. The SOC not only influences the semicore states of $5P$ Ce and $4d$ In, but also changes the density of states at the Fermi level $[\mathrm{DOS}(E_F)]$. The SOC splitting in the valance states is much smaller than the SOC splitting in the semicore states. However, the effects of the SOC would not be neglected in the results due to the fact that many physical quantities, e.g., EFG, are very sensitive to the value of the $\mathrm{DOS}(E_F)$. The latter point seems to be more significant for the Ce based compounds. A typical LDA/GGA calculation produces a sharp density of states for the $4f$ Ce, and situates it at the Fermi level. Thereby, any small changes in the sharply lo-

cated $4f$ Ce DOS at the Fermi level can change more significantly the DOS(E_F), and consequently the physical results.

The DOSs were also calculated for the ferromagnetic phase in the lack of SOC, which we call the "FM" phase. The result shows that imposing spin polarization (SP) causes the DOS(E_F) to be reduced from 141.82 states/Ry in the NM phase to 94.46 states/(spin Ry) for spin up and to 14.90 states/(spin Ry) for spin down in the FM phase. We have added up and down DOSs of the FM phase. Therefore a total reduction of 32.46 states/Ry in DOS(E_F) occurs in going from the NM to FM phase. Such a reduction affects the physical quantities that we shall discuss them in subsequent sections. We have then included the SOC in the FM phase, which we call the "FM+SOC" phase. The result shows that including SOC gives rise to a reduction of 14.60 states/Ry from FM to FM+SOC. The DOS(E_F) shows a total reduction of 47.06 states/Ry in going from NM to FM+SOC. Hence it seems that the SP and SOC can influence physical quantities in a similar direction in this compound.

The DOSs were calculated for the AFM state in the lack of SOC. The latter state is called the "AFM(001)" phase in this paper. In the absence of the SOC there is no preferred spatial direction at the cubic Ce site. In this case all the planes, for example, (111), (001), and so on, are identical. Thus for simplicity, the antiferromagnetic ordering, ($\uparrow\downarrow$), was aligned along the (001) axis. The SOC interactions were then included in the AFM(001) phase. One could introduce, at this step, a preferable direction in the presence of SOC. However, we would postpone setting up the correct direction of the cerium moments. The cerium moments were then kept still along the (001) axis, which we call the "AFM(001)+SOC" phase. The cerium moments in the AFM(111)+SOC phase were not changed to the more natural (111) direction in order to avoid mixing the effects of SOC with the effects of spin directions in the AFM phase. The result of AFM(001) or AFM(001)+SOC shows that the picks of the semicore Ce $5p$ and $4d$ In DOSs were nearly doubled in the AFM compared to the NM and FM phases. This is consistent with the fact that the number of electrons are doubled in going from the chemical cell to the magnetic supercell. We have then directed the $4f$ Ce spins from the (001) to (111) direction and recalculated the density of states self-consistently including spin-orbit coupling. The DOSs qualitatively were similar to those for the last case of the (001) direction. However, quantitatively only changing the direction changes the values of DOS(E_F) from 167.47 states/(spin Ry) to 127.98 states/(spin Ry) for the spin up, and from 167.24 states/(Ry spin) to 128.24 states/(spin Ry) for spin down. Such changes can affect the sensitive physical quantities.

We have included an appropriate correlation among $4f$ Ce electrons with employing LDA+U calculations. The $4f$ spin orientations were preserved antiferromagnetically along the (111) direction, and spin-orbit interactions were included in the LDA+U calculations. This constitutes our "AFM(111)+SOC+LDA+U" phase. Total DOSs of the AFM(111)+SOC+LDA+U phase are shown in Fig. 2. The result shows a significant reduction of the DOS(E_F) to 28.11 states/(spin Ry) for both up and down spins. Total

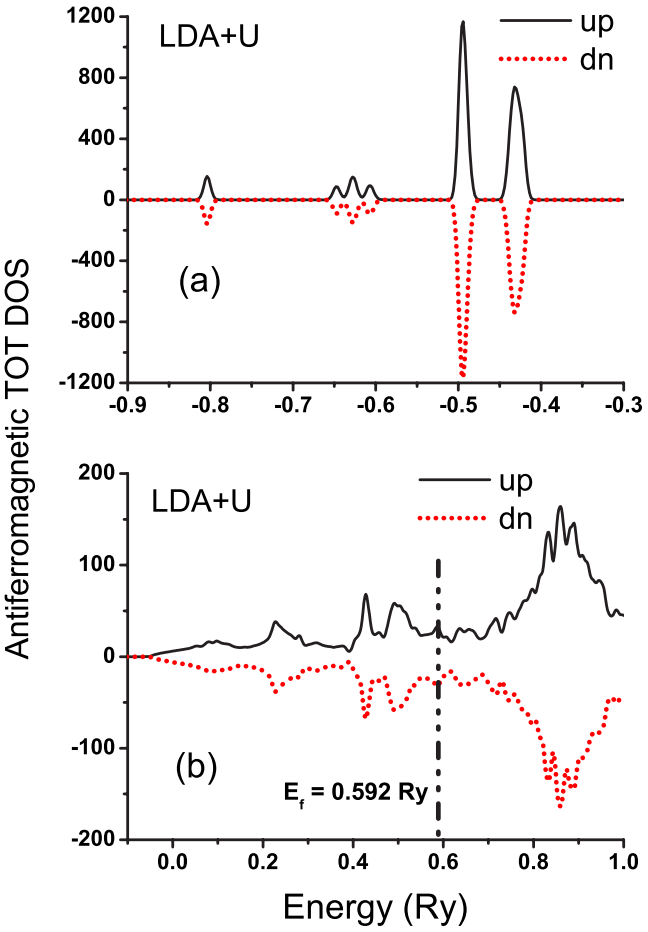

FIG. 2. (Color online) Total density of states of the AFM(111)+SOC+LDA+U phase presenting (a) semicore states and (b) valance states. The Fermi level is shown using a dashed line.

DOSs are separately illustrated in semicore, Fig. 2(a), and valance, Fig. 2(b), regions. The DOS of the semicore region shows further splitting in one of the branches of $5p$ Ce DOS. This occurs in comparison with the phase of AFM(111)+SOC. Our calculated total DOS of the latter phase, which is not shown here, is in complete accord with previous calculations.[3] One may confirm the above- mentioned further splitting by comparing Fig. 1 given in Ref. 3 with our Fig. 2(a). This shows that correlations among $4f$ electrons influence not only $4f$ Ce states directly, but also $5p$ Ce semicore states indirectly in this compound. There are two nonequivalent Ce atoms in the magnetic cell with opposite $4f$ spin directions, which are indexed as Ce1 and Ce2. The $4f$ DOSs of Ce1 and Ce2 are shown in Fig. 3 for both phases of AFM(111)+SOC and AFM(111)+SOC+LDA+U. The up and down $4f$-DOSs of Ce1 are asymmetric with respect to each other, which is the case for Ce2 as well. This is in the case that in overall Ce $4f$ DOS is entirely symmetric regardless of indexes 1 and 2. Therefore in spite of the fact that Ce1 and Ce2 can individually impose magnetic moment, no net magnetic moment is imposed in the whole of the supercell. The $4f$ DOS of the AFM(111)+SOC phase is also shown in Fig. 3(a). In this case one can more easily compare it with the latter phase of AFM(111)+SOC+LDA+U shown in Fig.

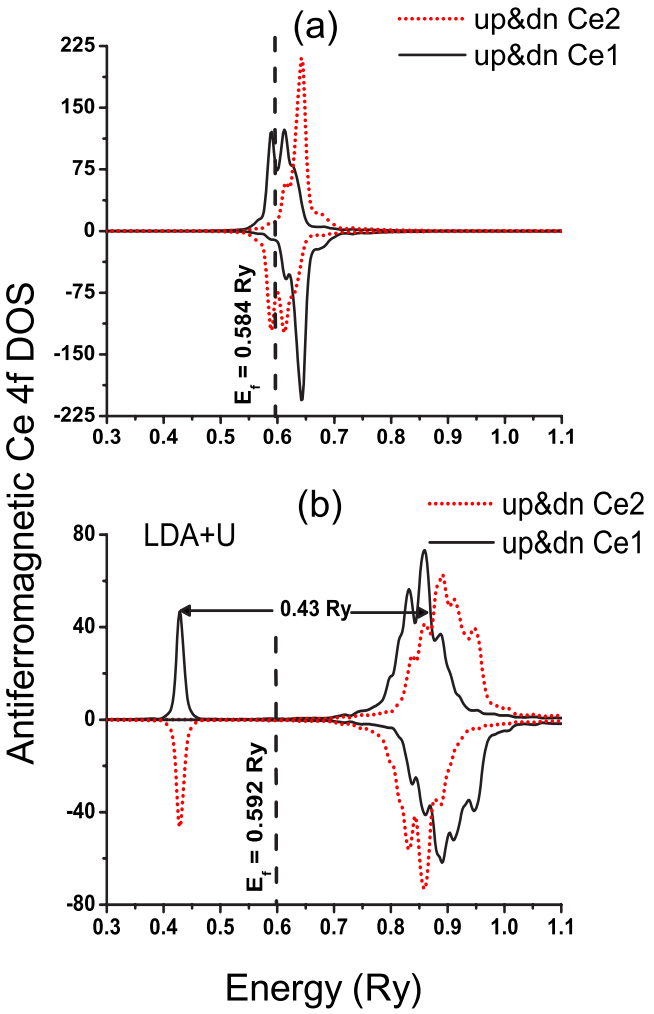

FIG. 3. (Color online) 4*f*-DOS of the (a) AFM(111)+SOC phase and (b) AFM(111)+SOC+LDA+U phase. Solid (dotted) curves show up and down DOS of the Ce1 (Ce2), where label 1 (2) refers to the attributed ↑ (↓) ordering. Fermi levels are shown using dashed lines for each of the cases.

3(b). The result shows that the significant reduction in the DOS(E_F) originates mainly from the splitting between occupied and unoccupied 4*f* bands; see Fig. 3(b). Such a splitting within LDA+U treatment is due to the effective Coulomb repulsion Hubbard *U* parameter. The 4*f* Ce DOS piles up in the vicinity of Fermi level within our GGA calculations. The latter point is what one can clearly see for the AFM(111)+SOC phase in Fig. 3(a). This is in the case that the LDA+U calculations give rise to be constituted with the 4*f* Ce DOS far from Fermi level. As shown in Fig. 3(b), including repulsion *U* potential energy causes to be shifted down occupied and shifted up unoccupied 4*f* DOS with respect to the Fermi level. The separation energy between upper and lower 4*f* bands is calculated to be 0.43 Ry. Thus contributions of 4*f* Ce to the value of DOS(E_F) are highly decreased. The receding of the 4*f* Ce DOS, from the vicinity of the Fermi level, indicates that the 4*f* electrons are going to lose their itinerant character, and as a result gain their localized character. In order to justify about the tendency of the 4*f* electrons to clarify the degree of their localization, one can compare Fig. 2(b) with Fig. 3(b). The comparison shows that the 4*f* Ce states play an important role and must not be ignored. The latter point may be deduced from two subsequent facts. First in energy space, the 4*f* states as shown in Fig. 3(b) are distributed over an energy interval for which other valence bands, e.g., In states, as shown in Fig. 2(b) are distributed as well. Second in real space, each In atom is surrounded by 4 Ce atoms as one can see in Fig. 1(a). Consequently, the 4*f* states are well-hybridized with the other valence bands even after including LDA+U. Thus the delocalization is reduced but not vanished by LDA+U. Therefore we conclude that not only bandlike treatment, but also open-core treatment cannot provide satisfactory results for the case of localized 4*f* states in this $CeIn_3$ compound. The former treatment would not be well-trusted because of putting 4*f* states right at the Fermi level. Thus the bandlike treatment overestimates hybridization of the 4*f* Ce states with the other valance states. The latter treatment would also not be well-trusted because of confining 4*f* states in the core region. Thus the open-core treatment usually underestimates hybridization of 4*f* Ce states with the other valance states.

IV. ELECTRONIC SPECIFIC HEAT

In this section, to fix ideas it seems advisable to compare the behavior of the electronic specific heats with the behavior of the DOS(E_F) through introduced phases in the preceding Sec. III C. The findings of this comparison in Sec. V will be of relevance to the goal of this paper to realize whether or not such a comparison can be generalized to the EFG quantity as well. Therefore we have plotted in Fig. 4(a) the calculated total and 4*f* Ce DOS(E_F) versus the discussed phases. The number of atoms in all the AFM phases is two times the number of other phases. The latter point is also the case for the DOS(E_F). We have then divided the DOS(E_F) by 2 for all the AFM phases. In this case, one can compare the AFM-DOS(E_F) with the DOS(E_F) of the other phases regardless of the number of atoms in the magnetic and chemical cells. One performing such a comparison can focus only on the magnetic ordering effects through all the defined various phases. The behavior of this curve constitutes the backbone of this paper.

We have calculated the electronic specific heats, C_V, in the absence of both phonon-phonon and electron-phonon interactions, and plotted the Sommerfeld linear coefficient, $\gamma = C_V/T$, in Fig. 4(b) versus all the phases. The result nicely represents the behavior of the total DOS(E_F) shown in Fig. 4(a), provided that the calculated specific heats per cell were also divided by 2 for the AFM phases. It is no surprise observing such a perfect consistency between on one side the behavior of the specific heats and on the other the behavior of DOS(E_F) going through our defined phases. The specific heats calculations were performed taking only electron-electron interactions into account. One can analytically omitting phonon interactions easily prove[29] the formula of $C_V/T = 1/3\pi^2 k_B^2 \mathrm{DOS}(E_F)$. This formula demonstrates a linear relation between γ and DOS(E_F). The above sketched strategy will numerically make an opportunity in the next

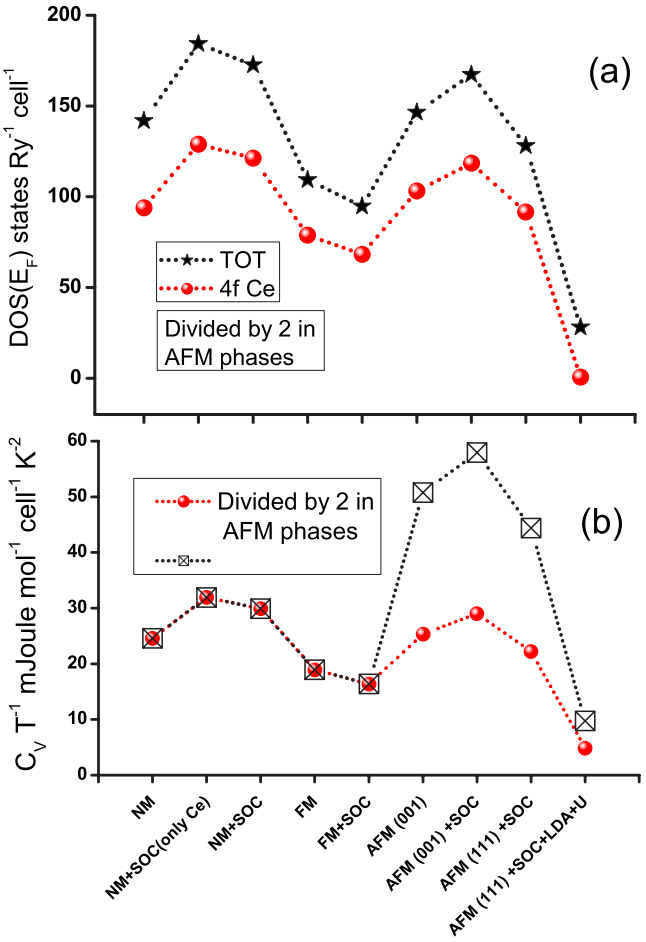

FIG. 4. (Color online) (a) Total and $4f$-Ce DOS versus a variety of phases discussed in the text at their respective Fermi levels. The values of DOS(E_F) are divided by 2 for all the AFM phases. (b) Sommerfeld linear coefficient $\gamma = C_V/T$ in mJ mol^{-1} cell^{-1} K^{-2} of the electronic specific heat shown by crossed squares versus all the phases. For comparison the γ coefficients, as shown by filled circles, are divided by 2 for the AFM phases.

section for trying to demonstrate an approximately linear relation between EFG and DOS(E_F). We close this section by reporting the value of 9.74 mJ/(mol cell K^2) within our LDA+U calculations. This calculated γ value is almost one order of magnitude less than the experimentally measured[30] value of 130 mJ/(mol cell K^2). The discrepancy is in agreement with all the other *ab initio* calculations for other cases in the lack of phonon interactions.[31–33]

V. ELECTRIC FIELD GRADIENT

The electric field gradient (EFG) is a tensor of rank 2. The EFG tensor has only two independent components in the principle axes system (PAS). The axes of the system were chosen such that $|V_{zz}| \geq |V_{yy}| \geq |V_{xx}|$. One can then only evaluate the main V_{zz} component of the EFG and the asymmetry parameter $\eta = \frac{V_{xx} - V_{yy}}{V_{zz}}$ to determine the two independent components of the EFG in the PAS. In this paper we only focus on the V_{zz} as our calculated electric field gradients, since the asymmetry parameters are zero for our case. The main component of the EFG tensor has been calculated using the following formula:[34]

$$V_{zz} = \lim_{r \to 0} \sqrt{\frac{5}{4\pi}} \frac{V_{20}}{r^2}, \tag{2}$$

where radial potential coefficient, V_{20}, within the LAPW method has been calculated as follows:[8,34]

$$V_{20}(r=0) = \frac{1}{5} \int_0^{R_{MT}} \frac{\rho_{20}}{r^3} \left\{ 1 - \left(\frac{r}{R_{MT}} \right)^5 \right\} d^3r + 4\pi \sum_K V(K) j_2(KR_{MT}) Y_{20}(\hat{K}). \tag{3}$$

The integral yields the EFG contribution of the electrons inside and over the surface of the muffin-thin sphere with a radius of R_{MT}. The summation yields the EFG contribution of the electrons entirely outside of the spheres. The contribution of the electrons inside the sphere is called the valance EFG, which we here denote by V_{zz}^{val}. The contribution of the electrons over the surface and outside of the spheres is called the lattice EFG, which we here denote by V_{zz}^{lat}.

Electric field gradients, V_{zz}'s, and their respective valance, V_{zz}^{val}'s, and lattice, V_{zz}^{lat}'s, components were calculated for all the introduced phases in Sec. III C. Our results are compared with experiment and other theoretical calculations in Table I. The anisotropy functions of $\Delta p(E_F)$ and $\Delta d(E_F)$ were also calculated and listed in Table II for all the phases. The result, in Table I, shows that our calculated EFG within the phase of AFM(111)+SOC+LDA+U is in better agreement with experiment than previous calculations.[1,3] The better agreement confirms that we have taken more properly into account correlations among $4f$ electrons within our LDA+U calculations. One observes, from Table II, that at the In site the absolute value of $\Delta p(E_F)$ is one order of magnitude greater than the absolute value of $\Delta d(E_F)$, which is not the case at the Ce site. For the latter case, the absolute value of $\Delta p(E_F)$ is one order of magnitude smaller than the absolute value of $\Delta d(E_F)$, i.e., $|\Delta p(E_F)| < |\Delta d(E_F)|$. We will get back to this point soon. What is important for us here is to study the variation of the EFG and appropriate anisotropy functions versus discussed phases to obtain a relation between EFG and DOS(E_F). Therefore we perform more comparisons throughout Tables I and II illustratively in Fig. 5. We have plotted V_{zz} in Fig. 5(a) and Δp in Fig. 5(b), both evaluated at the In site, versus all the phases. It is generally believed that contributions to the EFG originating from p states dominate.[34] Consequently, one expects to find a linear relation between EFG and Δp, i.e., EFG $\propto \Delta p$. This is what one expects to observe looking at Figs. 5(a) and 5(b). It is hard to realize, however, the linear relation of EFG $\propto \Delta p$ by comparing these two figures with each other. Therefore in order to exhibit such a linear relationship, we have separated three nonmagnetic phases from the other six magnetic phases. The V_{zz} and Δp were, respectively, shown in Figs. 5(c) and 5(d) versus three nonmagnetic phases. Similar results, V_{zz} and Δp, for the magnetic phases were separately shown in Figs. 5(e) and 5(f). Now one can among nonmagnetic phases clearly

TABLE I. The main component of the EFG, V_{zz}, and its decomposition to valance, V_{zz}^{val}, and lattice, V_{zz}^{lat}, components given in the units of 10^{21} V/m^2 at both In and Ce sites for all the phases discussed in the text together with the calculated results within the LAPW method by the others as well as experimental EFG.

	Inte.			V_{zz}		V_{zz}^{val}		V_{zz}^{lat}	
Phase	SOC	LDA+U	$\vec{M}^{\parallel}$	In	Ce	In	Ce	In	Ce
NM	No	No		13.209	0	13.263	0	−0.054	0
NM	Only Ce	No		12.466	0	12.515	0	−0.049	0
NM	Yes	No		12.847	0	12.538	0	−0.051	0
FM	No	No		13.018	0	13.024	0	−0.006	0
FM	Yes	No	(001)	12.843	0.082	12.867	0.105	−0.024	−0.023
AFM	No	No	(001)	13.027	0.089	13.032	0.086	−0.005	−0.003
AFM	Yes	No	(001)	12.966	0.086	12.968	0.066	−0.002	−0.002
AFM	Yes	No	(111)	12.857	0.029	12.961	0.040	−0.004	−0.011
AFM	Yes	Yes	(111)	12.431	−2.863	12.442	−2.889	−0.011	0.026
[a]AFM	Yes	No	(111)	12.490		12.540		−0.050	
[b]AFM^{exp}			Unknown	11.6					

[a]Reference 3.
[b]Reference 1.

observe the linear relation between EFG and Δp by comparing the behavior of V_{zz}, Fig. 5(c), with the behavior of Δp shown in Fig. 5(d). They behave similar to each other through nonmagnetic phases. This is also the case for the magnetic phases as well, since the V_{zz} shown in Fig. 5(e) behaves similar to Δp shown in Fig. 5(f) through the magnetic phases. Now the time seems apt to intuit that there is an approximately linear relation between EFG and DOS(E_F), i.e., EFG$\propto$DOS(E_F). The relation can be realized if the behavior of the total DOS(E_F) shown in Fig. 4(a) is compared with the behavior of the V_{zz} shown in Figs. 5(c) and 5(e). The comparison yields the result that the EFG is approximately proportional to the DOS(E_F). The result is obtained because the V_{zz} and the DOS(E_F) vary similarly, going through all the phases. This is analogous to the used strategy in Sec. IV to realize the linear relation of $C_V/T=1/3\pi^2k_B^2$DOS(E_F). Our result shows that the proportional constant is negative for the nonmagnetic phases, while it is positive for the magnetic phases. The former constant is negative because the V_{zz} and DOS(E_F) inversely vary through nonmagnetic phases. They, however, vary directly versus magnetic phases resulting in the positive constant.

Furthermore, one can also conclude that the value of $4f$-DOS(E_F) can significantly influence the value of EFG. One may confirm this conclusion due to a similarity between the behavior of $4f$DOS(E_F) and total DOS(E_F) shown in Fig. 4(a). The foregoing result of EFG$\propto$DOS(E_F) ensures that the EFG can be also proportional to the $4f$DOS(E_F); i.e., EFG $\propto$DOS^{4f}(E_F).

The latter proportionality between EFG and $4f$DOS(E_F) makes more crucial the method of treatment with $4f$-Ce electrons. The latter point describes why the value of EFG at the In site within the LDA+U calculation is smaller than those obtained within all the other calculations performed in the lack of LDA+U interactions. The description can be provided taking the splitting of 0.43 Ry shown in Fig. 3(b) into

TABLE II. Valance p and d anisotropy functions, $\Delta p(E_F)$ and $\Delta d(E_F)$, evaluated at In and Ce sites for the discussed phases in the text.

	Inte.			Δp		Δd	
Phase	SOC	LDA+U	$\vec{M}^{\parallel}$	In	Ce	In	Ce
NM	No	No		0.1066	0	−0.0060	0
NM	Only Ce	No		0.1040	0	−0.0061	0
NM	Yes	No		0.1043	0	−0.0061	0
FM	No	No		0.0373	0	−0.0050	0
FM	Yes	No	(001)	0.0369	0	−0.0052	0
AFM	No	No	(001)	0.0373	0.00015	0.0025	0.00130
AFM	Yes	No	(001)	0.0372	0.00005	0.0024	0.00130
AFM	Yes	No	(111)	0.0370	−0.00010	0.0024	−0.00085
AFM	Yes	Yes	(111)	0.0361	0.00715	0.0026	0.01880

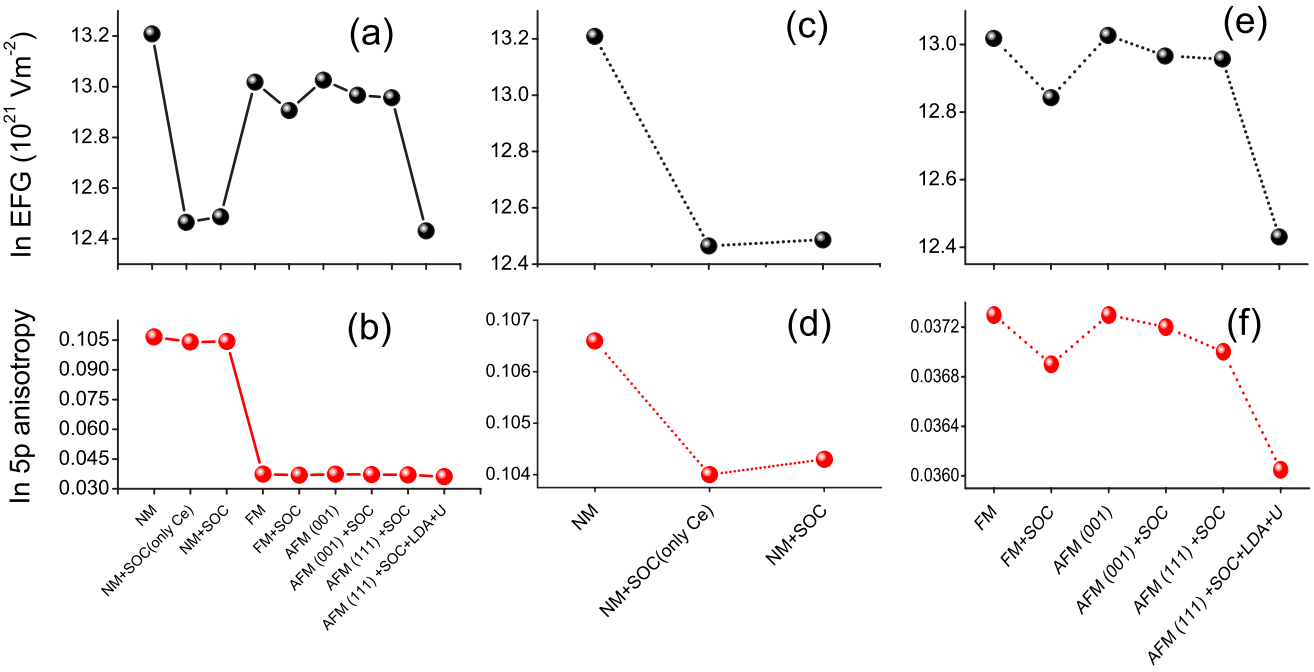

FIG. 5. (Color online) (a) The calculated EFG at the In site and (b) the In 5p anisotropy function, $\Delta p(E_F)$, for all the nonmagnetic and magnetic phases discussed in the text. They are also represented in (c) and (d) for only nonmagnetic phases as well as in (e) and (f) for only magnetic phases.

account between occupied and unoccupied bands due to the LDA+U treatment. The splitting gives rise to be shifted downwards of the 4f DOS from the vicinity of Fermi level, and as a result to be reduced to the value of 4fDOS(E_F). The latter reduction together with the discussed relation of EFG $\propto$DOS$^{4f}(E_F)$ provides the satisfactory description why the EFG is reduced within LDA+U calculations. All these support our previously concluded result in Sec. III C concerning the important role of 4f electrons in this compound.

At the Ce site due to its cubic point group the EFGs are zero, as listed in Table I, for all nonmagnetic phases and FM phase. For the FM+SOC phase and all the AFM phases, however, our result shows nonzero EFG values at this site. The nonzero values for the EFGs originate from the fact that SOC or magnetic ordering can give rise to a little bit of deviation from cubic symmetry. One expects that the small deviation gives rise to small EFGs. Our result, in Table I, confirms the latter point apart from the last phase of AFM(111)+SOC+LDA+U. For the latter AFM(111) +SOC+LDA+U phase the EFG at the Ce site is also practically small, but it is two orders of magnitude larger than the other phases. To find the source of such a discrepancy, we follow our last strategy looking at the behavior of EFG and anisotropy functions through corresponded phases. The calculated EFG at the Ce site can be compared with the Δp versus magnetic phases (apart from the FM phase for which EFG is exactly zero) using Figs. 6(a) and 6(b). The comparison does not show similar behavior for the EFG and Δp along the magnetic phases. To find the reason why they do not show similar behavior, now we come back to the mentioned point that $|\Delta d(E_F)| > |\Delta p(E_F)|$ at the Ce site; see Table II. One first suspects, due to the larger value of $|\Delta d(E_F)|$ than $|\Delta p(E_F)|$, that the behavior of EFG might be similar to the behavior of $\Delta d(E_F)$. The behaviors of EFG and $\Delta d(E_F)$ are compared in Figs. 6(a) and 6(c). However, they also do not show similar behavior. Therefore we could not reproduce the behavior of the EFG using either $\Delta p(E_F)$ or $\Delta d(E_F)$. For more realization, we have decomposed the EFG at the Ce site into its valance contributions. The results, the sum of up and down spins, are shown in Fig. 7 for each of the valance contributions. The result, comparing Figs. 7(a) and 7(b), shows that contributions of d-states to the EFG is one order of magnitude less than contributions of p-states. This is in the case that, as expressed before, $|\Delta d(E_F)|$ is one order of magnitude larger than $|\Delta p(E_F)|$. Therefore even for the case of $|\Delta d(E_F)| > |\Delta p(E_F)|$, contributions to the EFG originating from p-states compared to the d-states dominate. This result is in complete accord with the calculations performed in Ref. 34 for transition metals. However, a different and important result can emerge from comparing Fig. 7(c) with Fig. 6(a). The result is that the EFG mainly originates from f-states at the Ce site. We have added all the valance contributions to the EFG in Fig. 7(d). The result shows that the behavior of EFG shown in Fig. 6(a) is similar to total valance EFG contributions shown in Fig. 7(d). Lattice contributions to the EFG also cannot change the similarity because they are negligible as listed in Table I. Therefore contributions to the EFG originating from f-states dominate at the Ce site.

VI. CONCLUSION

We have investigated the variations of electric field gradients (EFGs) and their valance contributions as well as their anisotropy functions at both In and Ce sites in the $CeIn_3$ for

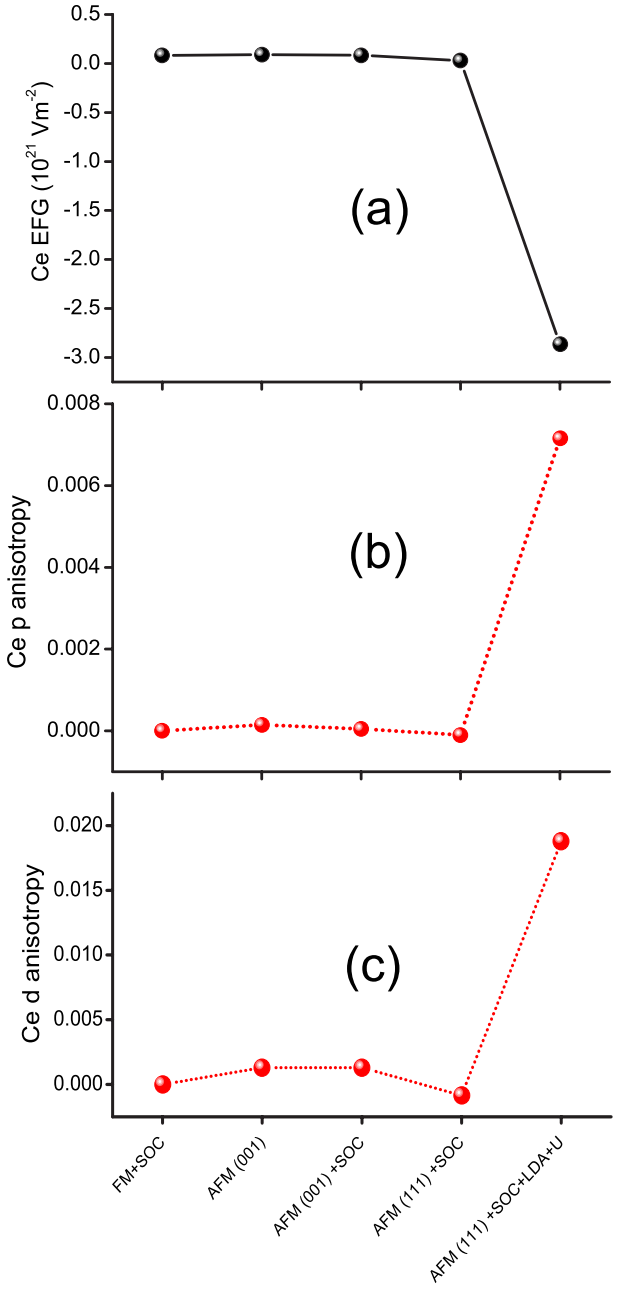

FIG. 6. (Color online) (a) The calculated EFG at the Ce site, (b) the Ce p anisotropy function, $\Delta p(E_F)$, and (c) the Ce d anisotropy function, $\Delta d(E_F)$, for the phases discussed in the text for which nonzero EFGs have been calculated at the Ce site, viz. ranging from FM+SOC to AFM(111)+SOC+LDA+U.

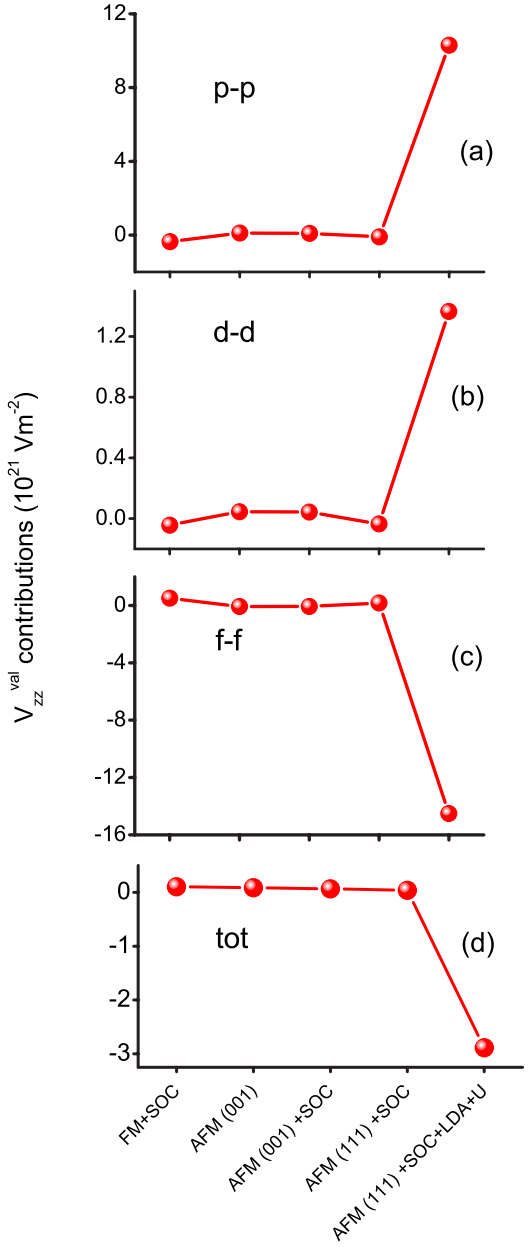

FIG. 7. (Color online) (a) Up plus down valance contributions of EFG evaluated at the Ce site for the magnetic phases discussed in the text ranging from FM+SOC to AFM(111)+SOC+LDA+U. (There are no EFG contributions at the Ce site for the FM phase, in the lack of SOC, due to its cubic symmetry.)

a variety of circumstances. For each of the circumstances, density of states at Fermi level [DOS(E_F)] is calculated. We have found that comparing the behavior of the EFG with the behavior of DOS(E_F) versus the applied circumstances may be a useful strategy to emerge physical properties. We have found within such a strategy that the main component of the electric field gradient, V_{zz}, is approximately proportional to the value of total density of states at Fermi level [DOS(E_F)] as well as $4f-\mathrm{DOS}(E_F)$. Despite that the anisotropy function of d-states is larger than the one of p-states at the Ce site, contributions to the EFG originating from p-states dominate compared to d-states. This is in the case that, however, the EFGs are dominated at the Ce site by the $4f$-states, while they are as usual dominated by p-states at the In site. The result shows that $4f$ Ce states are hybridized with valence bands and play an important role which must not be ignored. Thus we have within our electronic structure calculations predicted that neither bandlike treatment, nor open-core treatment can provide satisfactory results for this case. Our

LDA+U calculations are in better agreement with experiment indicating the fact that correlations among 4*f* electrons are taken more properly into account. The correlations among 4*f* electrons influence not only 4*f* Ce states directly, but also 5*p* Ce semicore states indirectly in this compound.

ACKNOWLEDGMENT

This work has been performed based on the research project number 821235, University of Isfahan (UI), Isfahan, Iran.

*Electronic address: sjalali@phys.ui.ac.ir

[1] Y. Kohori, Y. Inoue, T. Kohara, G. Tomka, and P. C. Riedi, Physica B **259-261**, 103 (1999).
[2] Y. Kohori, T. Kohara, Y. Yamato, G. Tomka, and P. C. Riedi, Physica B **281-282**, 12 (2000).
[3] M. V. Lalić, J. Mestnik-Filho, A. W. Carbonari, R. N. Saxena, and H. Haas, Phys. Rev. B **65**, 054405 (2001).
[4] K. Betsuyaku and H. Harima, J. Magn. Magn. Mater. **272-276**, 187 (2004).
[5] J. M. Lawrence and S. M. Shapiro, Phys. Rev. B **22**, 4379 (1980); J. P. Morin, C. Vettier, J. Flouquet, M. Konczykowsky, Y. Lassailly, J. M. Mignot, and U. Welp, J. Low Temp. Phys. **70**, 377 (1988); B. Benoit, J. X. Boucherle, P. Convert, J. Flouquet, J. Palleau, and J. Schweizer, Solid State Commun. **34**, 293 (1980).
[6] N. D. Mathur, F. M. Grosche, S. R. Julian, I. R. Walker, D. M. Freye, R. K. W. Haselwimmer, and G. G. Lonzarich, Nature (London) **394**, 39 (1998).
[7] J. Yu, A. J. Freeman, R. Podloucky, P. Herzig, and P. Weinberger, Phys. Rev. B **43**, 532 (1991).
[8] K. Schwarz, C. Ambrosch-Draxl, and P. Blaha, Phys. Rev. B **42**, 2051 (1990).
[9] J. Rusz and M. Biasini, Phys. Rev. B **71**, 233103 (2005).
[10] S. J. Asadabadi, S. Cottenier, H. Akbarzadeh, R. Saki, and M. Rots, Phys. Rev. B **66**, 195103 (2002).
[11] S. Jalali Asadabadi and H. Akbarzadeh, Physica B **349**, 76 (2004).
[12] D. J. Singh and L. Nordström, *Planewaves, Pseudopotentials, and the LAPW Method*, 2nd ed. (Springer, New York, 2006), Vol. XIII, p. 134.
[13] V. I. Anisimov and O. Gunnarsson, Phys. Rev. B **43**, 7570 (1991).
[14] V. I. Anisimov, I. V. Solovyev, M. A. Korotin, M. T. Czyżyk, and G. A. Sawatzky, Phys. Rev. B **48**, 16929 (1993).
[15] M. T. Czyżyk and G. A. Sawatzky, Phys. Rev. B **49**, 14211 (1994).
[16] E. Sjöstedt, L. Nordström, and D. J. Singh, Solid State Commun. **114**, 15 (2000).
[17] G. K. H. Madsen, P. Blaha, K. Schwarz, E. Sjöstedt, and L. Nordström, Phys. Rev. B **64**, 195134 (2001).
[18] P. Hohenberg and W. Kohn, Phys. Rev. **136**, A864 (1964).
[19] W. Kohn and L. J. Sham, Phys. Rev. **140**, A1133 (1965).
[20] J. P. Perdew, K. Burke, and M. Ernzerhof, Phys. Rev. Lett. **77**, 3865 (1996).
[21] P. Blaha, K. Schwarz, G. K. H. Madsen, D. Kvasnicka, and J. Luitz, *WIEN2k, An Augmented Plane* Wave+Local *Orbitals Program for Calculating Crystal Properties* (Karlheinz Schwarz, Techn. Universitat Wien, Austria, 1999).
[22] H. J. Monkhurst and J. D. Pack, Phys. Rev. B **13**, 5188 (1976).
[23] D. D. Koelling and B. N. Harmon, J. Phys.: Condens. Matter **10**, 3107 (1997).
[24] A. H. MacDonald, W. E. Pickett, and D. D. Koelling, J. Phys. C **13**, 2675 (1980); Lecture note of Pavel Novak (1997) on Spin-Orbit Coupling available from: http://www.wien2k.a/reg_user/textbooks/novak_lecture_on_spinorbit.ps; see also Ref. 12.
[25] N. Kioussis, J. Thevenot, B. R. Cooper, and Q. G. Sheng, J. Appl. Phys. **79**, 6420 (1996).
[26] A. B. Shick, W. E. Pickett, and A. I. Liechtenstein, arXiv:cond-mat/0001255v1 (unpublished).
[27] H. Sawada, Y. Morikawa, K. Terakura, and N. Hamada, Phys. Rev. B **56**, 12154 (1997); S. L. Dudarev, G. A. Botton, S. Y. Savrasov, C. J. Humphreys, and A. P. Sutton, *ibid.* **57**, 1505 (1998).
[28] I. R. Harris and G. V. Raynor, J. Less-Common Met. **9**, 7 (1965).
[29] C. Kittle, *Introduction to Solid State Physics*, 8th ed. (Wiley, Hoboken, NJ, 2005), Chap. 6, p. 144.
[30] S. Nasu, A. M. van Diepen, H. H. Neummann, and R. S. Craig, J. Phys. Chem. Solids **32**, 2772 (1971); M. Nicklas, R. Borth, E. Lengyel, P. G. Pagliuso, J. L. Sarrao, V. A. Sidorov, G. Sparn, F. Steglich, and J. D. Thomson, J. Phys.: Condens. Matter **13**, L905 (2001).
[31] L. Petit, A. Svane, W. M. Temmerman, Z. Szotek, and R. Tyer, Europhys. Lett. **62**, 391 (2003).
[32] R. C. Albers, A. M. Boring, and N. E. Christensen, Phys. Rev. B **33**, 8116 (1986).
[33] M. M. Steiner, R. C. Albers, and L. J. Sham, Phys. Rev. Lett. **72**, 2923 (1994).
[34] P. Blaha, K. Schwarz, and P. H. Dederichs, Phys. Rev. B **37**, 2792 (1988).